

Article

Synthesis, Structure and Bonding in Pentagonal Bipyramidal Cluster Compounds Containing a *cyclo*-Sn₅ Ring, [(CO)₃MSn₅M(CO)₃]⁴⁻ (M = Cr, Mo)

Sourav Mondal ^{1,†} , Wei-Xing Chen ^{2,†} , Zhong-Ming Sun ^{2,*}  and John E. McGrady ^{1,*} 

¹ Department of Chemistry, University of Oxford, South Parks Road, Oxford OX1 3QZ, UK; sourav.mondal@chem.ox.ac.uk

² State Key Laboratory of Elemento-Organic Chemistry, Tianjin Key Lab of Rare Earth Materials and Applications, School of Material Science and Engineering, Nankai University, Tianjin 300350, China; 1120200450@mail.nankai.edu.cn

* Correspondence: sunlab@nankai.edu.cn (Z.-M.S.); john.mcgrady@chem.ox.ac.uk (J.E.M.)

† These authors contributed equally to this work.

Abstract: In this paper, we report the synthesis and structural characterisation of two hetero-metallic clusters, [(CO)₃CrSn₅Cr(CO)₃]⁴⁻ and [(CO)₃MoSn₅Mo(CO)₃]⁴⁻, both of which have a pentagonal bipyramidal core. The structures are similar to that of previously reported [(CO)₃MoPb₅Mo(CO)₃]⁴⁻ and our analysis of the bonding suggests that they are best formulated as containing Sn₅⁴⁻ rings bridging two zerovalent M(CO)₃ fragments. The electronic structure is compared to two isolobal M₂E₅ clusters, [CpCrP₅CrCp]⁻ and Tl₇⁷⁻, both of which show clear evidence for *trans*-annular bonds between the apical atoms that is not immediately obvious in the title clusters. Our analysis shows that the balance between E-E and M-M bonding is a delicate one, and shifts in the relative energies of the orbitals on the E₅ and M₂ fragments generate a continuum of bonding situations linked by the degree of localisation of the cluster LUMO.

Keywords: Zintl clusters; X-ray crystallography; Density Functional Theory



Citation: Mondal, S.; Chen, W.-X.; Sun, Z.-M.; McGrady, J.E. Synthesis, Structure and Bonding in Pentagonal Bipyramidal Cluster Compounds Containing a *cyclo*-Sn₅ Ring, [(CO)₃MSn₅M(CO)₃]⁴⁻ (M = Cr, Mo). *Inorganics* **2022**, *10*, 75. <https://doi.org/10.3390/inorganics10060075>

Academic Editor: Duncan H.

Gregory

Received: 11 May 2022

Accepted: 26 May 2022

Published: 30 May 2022

Publisher's Note: MDPI stays neutral with regard to jurisdictional claims in published maps and institutional affiliations.



Copyright: © 2022 by the authors. Licensee MDPI, Basel, Switzerland. This article is an open access article distributed under the terms and conditions of the Creative Commons Attribution (CC BY) license (<https://creativecommons.org/licenses/by/4.0/>).

1. Introduction

The chemistry of *cyclo*-Pn₅ rings of the pnictogens is now well established, and many coordination compounds of P₅⁻ and its heavier congeners, As₅⁻ and Sb₅⁻, have been reported in the literature [1–3]. These are of interest from a synthetic perspective, but also in the context of the isolobal relationship between Pn and CH [4,5] which can be used, for example, to rationalise the very similar structural chemistry of complexes of P₅⁻ and C₅H₅⁻ [6]. Rather less common are *cyclo*-Tt₅ rings containing the tetrel elements Si, Ge, Sn and Pb. An isoelectronic relationship to P₅⁻ would require a formal charge of -6, and indeed Todorov and Sevov have reported both Sn₅⁶⁻ and Pb₅⁶⁻ in a family of Zintl phases, Na₈BaPb₆, Na₈BaSn₆ and Na₈EuSn₆, Figure 1, (where charge balance is maintained by the presence of an isolated Tt⁴⁻ ion in the unit cell in addition to a Tt₅⁶⁻ ring) [7]. Lighter homologues such as Si₅⁶⁻ and Ge₅⁶⁻ have an even longer history, having been identified in binary phases such as Li₁₂Si₇ and Li₁₁Ge₆ as far back as the late 1970s [8–10]. The stability of the planar Tt₅⁶⁻ rings can be rationalised either on the grounds of aromaticity (the rings have 6 π electrons), or in terms of Wade's rules (the clusters have a 2n + 6 = 16 skeletal electron count or, equivalently, a total valence electron count of 4n + 6 = 26, consistent with a 5-vertex *arachno* cluster based on a pentagonal bipyramid with two missing *trans* vertices) [11]. These two perspectives, both equally valid, highlight the important point that the bonding in ring and cluster compounds of the heavier main group elements is complex, and different interpretations are often possible.

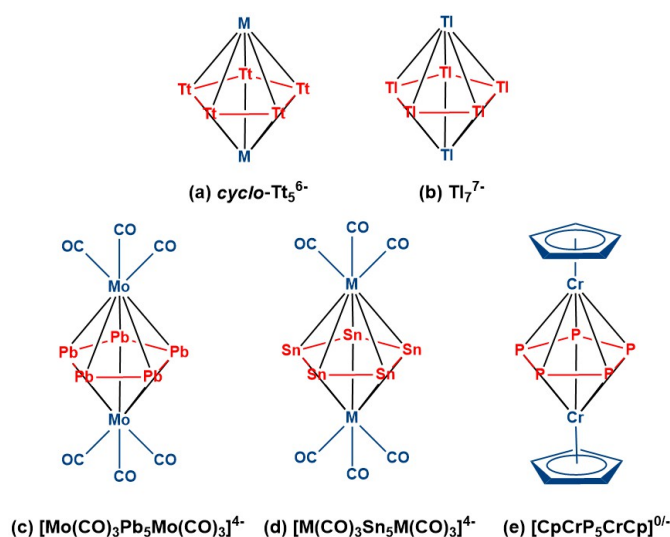


Figure 1. Examples of pentagonal bipyramidal cluster architectures from the transition metal series and main-group: (a) cyclo-Tt_5^{6-} ($\text{Tt} = \text{Si}, \text{Sn}, \text{Pb}$; $\text{M} = \text{alkali, alkaline- or rare-earth metals}$); (b) Tl_7^{7-} in the binary phase K_{10}Tl_7 [12]; (c) $[(\text{CO})_3\text{MoPb}_5\text{Mo}(\text{CO})_3]^{4-}$ [13], (d) $[(\text{CO})_3\text{MSn}_5\text{M}(\text{CO})_3]^{4-}$ ($\text{M} = \text{Cr}, \text{Mo}$), this work and (e) $[\text{CpCrP}_5\text{CrCp}]^{0/-}$ [14].

Soon after Sevov's report of the Sn_5^{6-} and Pb_5^{6-} rings [7], Fässler, Kaupp and co-workers described the synthesis of a molecular analogue, $[(\text{CO})_3\text{MoPb}_5\text{Mo}(\text{CO})_3]^{4-}$, which they formulated as a Pb_5^{4-} ring bridging two neutral $\text{Mo}(\text{CO})_3$ fragments [13]. The 4π electron count is now consistent with anti-aromatic, rather than aromatic, character, but the Pb-Pb bond lengths in this cluster (3.0138–3.0647 Å) are nevertheless marginally shorter than those in the aromatic (6π) Pb_5^{6-} unit in Na_8BaPb_6 (3.047–3.117 Å). An analysis of the electronic structure reveals very substantial transfer of charge from the Pb_5^{4-} ring to the $\text{Mo}(\text{CO})_3$ fragments, such that the most intense C-O stretching frequency (1737 cm^{-1}) is substantially reduced from the value of 1960 cm^{-1} in the precursor, (mesitylene) $\text{Mo}(\text{CO})_3$ [15], and this covalency clearly precludes a simple correlation between bond lengths and formal charge on the five-membered ring. Gholiee et al. have, more recently, published a detailed computational survey of the family of pentagonal bipyramidal clusters with general formula $[(\text{CO})_3\text{ME}_5\text{M}(\text{CO})_3]^{4-}$, $\text{M} = \text{Cr}, \text{Mo}, \text{W}$, $\text{E} = \text{Si}, \text{Ge}, \text{Sn}$ and Pb [16]. Their analysis, using the M06-2X functional in combination with a def2-TZVPP basis, concurs with the conclusion from Fässler and Kaupp, that there is substantial charge transfer from the formally Tt_5^{4-} ring to the $\text{M}(\text{CO})_3$ fragments, such that the former actually carries a positive natural charge: clearly the formal charge is at best a first approximation, and the balance between M-M, M-Tt and Tt-Tt bonding is a delicate one.

In this paper, we report the synthesis and structural characterisation of two tin analogues of Fässler's lead cluster, $[(\text{CO})_3\text{MSn}_5\text{M}(\text{CO})_3]^{4-}$, $\text{M} = \text{Cr}$ (1) and Mo (2), both of which were included in Gholiee's computational survey [16]. Both compounds are formed from the reaction of K_4Sn_9 with the organometallic precursors $\text{M}(\text{MeCN})_3(\text{CO})_3$ ($\text{M} = \text{Cr}, \text{Mo}$), and both feature a planar cyclo-Sn_5 motif capped by two $\text{M}(\text{CO})_3$ fragments. This new structural data provides a platform to consider the general features of bonding in the family of pentagonal bipyramids. In the final section of this paper, we take the opportunity to compare these two new clusters to closely related species that share the pentagonal bipyramidal architecture, and to compare the different electron-counting models that have been applied in this context.

2. Materials and Methods

All manipulations and reactions were performed under a dry nitrogen atmosphere in the glove box. Ethylenediamine (en) (99%, Sigma-Aldrich, Beijing, China), and N, N-Dimethylformamide (Sigma-Aldrich, 99.8%) were freshly distilled and

stored under nitrogen before use. Toluene (Sigma-Aldrich, 99.8%) was distilled from sodium/benzophenone under nitrogen and stored under nitrogen. The [2.2.2]crypt (4,7,13,16,21,24-Hexaoxa-1,10-diazabicyclo (8.8.8) hexacosane) (98%), and 18-Crown-6 (1,4,7,10,13,16-Hexaoxacyclooctadecane) (99%), both purchased from Sigma-Aldrich, were dried in vacuum for 12 h prior to use. K_4Sn_9 was synthesised by heating a mixture of K and Sn (K: 99%, Sn: 99.99%, both from Aladdin (Shanghai, China)) at 850 °C for 48 h in a tubular tantalum container and then cooling to room temperature at a rate of 10 °C/h. Finally, black powders were obtained. The $M(MeCN)_3(CO)_3$ ($M = Cr, Mo$) starting materials were synthesised according to literature procedures [17].

2.1. Synthesis of $K_2(en)_3[K([2.2.2]-crypt)]_2[Cr(CO)_3Sn_5Cr(CO)_3].2en$, (**1**)

K_4Sn_9 (100 mg, 0.817 mmol) and [2.2.2]crypt (150 mg, 0.399 mmol) were dissolved in 3 mL en solution in a 10 mL vial, and the mixture was stirred vigorously for 30 min at room temperature. The organometallic precursor $Cr(MeCN)_3(CO)_3$ (30 mg 0.116 mmol) was then added and stirring continued for 3 h at room temperature. The resulting red-brown solution was centrifuged and filtered with standard glass wool, then carefully layered with 3 mL toluene. After 5 days, small dark-brown needle-like crystals of **1** (Figure S1, left) were observed in the bottom of the test tube in approximately 26% yield (based on precursor $Cr(MeCN)_3(CO)_3$ used).

2.2. Synthesis of $K[K(18-crown-6)]_3[Mo(CO)_3Sn_5Mo(CO)_3]$ (**2**)

K_4Sn_9 (100 mg, 0.817 mmol) and 18-Crown-6 (105 mg, 0.397 mmol) were dissolved in 3 mL en solution in a 10 mL vial, and the mixture was stirred vigorously for 30 min at room temperature. The organometallic precursor $Mo(MeCN)_3(CO)_3$ (35 mg 0.116 mmol) was then added and stirring continued for 4 h at room temperature. The resulting red-brown solution was centrifuged and filtered with standard glass wool, then carefully layered with 3 mL toluene. After 7 days, dark-brown needle-like crystals of **2** (Figure S1, right) were observed in the bottom of the test tube in approximately 19% yield (based on precursor $Mo(MeCN)_3(CO)_3$ used).

2.3. X-ray Diffraction

Suitable crystals of **1** and **2** were selected for X-ray diffraction analyses. Crystallographic data were collected on Rigaku XtalAB Pro MM007 DW diffractometer with graphite monochromated Cu $K\alpha$ radiation ($\lambda = 1.54184 \text{ \AA}$). The structures of crystals **1** (Figures S2 and S3) and **2** (Figures S4 and S5) were solved using direct methods and then refined using SHELXL-2014 and OLEX2 [18,19]. All the non-hydrogen atoms were refined anisotropically, except for those in the split positions. The uncoordinated solvent molecules in **1** and **2** could not be modeled properly, so the solvent molecules are removed using SQUEEZE in PLATON [20]. The cluster anion in **1** has a disordered structure which was solved by the Split SAME process [19]. The unique bond angles and distances were constrained by Dfix order. We use the SIMU order to limit the anisotropic displacement parameters of the interconnected atoms to be similar. A summary of the crystallographic data for the title compounds is listed in Table S1, and selected bond distances and bond angles are given in Table S2. CCDC entries CCDC-2122111 and CCDC-2122112 for compounds **1** and **2** contain the supplementary crystallographic data for this paper. These data can be obtained free of charge via www.ccdc.cam.ac.uk/data_requested/cif (accessed on 15 November 2021).

2.4. Electrospray Ionisation Mass Spectrometry (ESI-MS)

Negative ion mode ESI-MS of a MeCN solution made up from crystals of **1** were measured on an LTQ linear ion trap spectrometer by Agilent Technologies ESI-TOF-MS (6230). The spray voltage was 5.48 kV and the capillary temperature was maintained at 300 °C. The capillary voltage was 30 V. The samples were prepared inside a glove box and

very rapidly transferred to the spectrometer in an airtight syringe by direct infusion with a Harvard syringe pump at 0.2 mL/min.

2.5. Energy Dispersive X-ray (EDX) Analysis

EDX analysis was performed to support the elemental composition proposed in the XRD experiment. These were carried out using a scanning electron microscope (Hitachi S-4800) equipped with a Bruker AXS XFlash detector 4010. Data acquisition was performed with an acceleration voltage of 20 kV and an accumulation time of 150 s (Figures S8 and S9).

2.6. Computational Details

All DFT calculations were performed using the ORCA 5.0.1 software [21,22]. A range of functionals was considered, including the generalised gradient approximation (GGA) functional proposed by Perdew, Burke and Ernzerhof (PBE) [23], the hybrid B3LYP [24–26], the meta-hybrid M06-2X [27] and the double-hybrid, B2PLYP [28,29]. Scalar relativistic effects were included using the zeroth-order relativistic approximation (ZORA) [30–32]. A valence triple-zeta polarised relativistically recontracted Karlsruhe basis set (ZORA-def2-TZVP) [33–35] was employed for H, C and O and segmented all-electron relativistically contracted (SARC) basis sets were used for heavier elements. The RI-J approximation to the Coulomb integrals (J) was made using the (SARC/J) [34–36] auxiliary basis set appropriate for ZORA calculations. The conductor-like polarisable continuum mode (CPCM) was implemented taking water as a solvent with dielectric constant (ϵ) 80.4 to model the confining potential of the cation lattice [37–40]. The multiwfn package was used to analyse the topology of the electron density and to compute bond orders [41]. Graphics containing molecular structures were generated using Chemcraft [42].

3. Results

3.1. Synthesis and Structural Characterisation

The synthesis of both **1** and **2** was achieved by reacting a transition metal carbonyl precursor, $M(\text{MeCN})_3(\text{CO})_3$, with K_4Sn_9 in the presence of a chelating ligand, 18-Crown-6 or [2.2.2]-crypt, that binds K^+ cations in the final product. In initial tests, both chelating ligands were used with both transition metals, but in the case of 18-Crown-6 with Cr or [2.2.2]-crypt with Mo, the major products were the known clusters $[\text{M}(\text{CO})_3\text{Sn}_9]^{4-}$ [43], rather than the Sn_5 -containing species. The influence of the chelating ligand most likely reflects subtle differences in the solubility of the two competing anions with cations of different size. X-ray diffraction analysis reveals that **1** crystallises in the triclinic space group $\text{P}\bar{1}$ and contains a $[(\text{CO})_3\text{CrSn}_5\text{Cr}(\text{CO})_3]^{4-}$ anion with two isolated K^+ ions and two $[\text{K}([2.2.2]\text{-crypt})]^+$ cations per cluster (Figures S2 and S3). The anionic clusters are arranged in approximately linear chains, with the K^+ ions bridging adjacent units via four $\text{K}^+\text{-O}(\text{CO})$ contacts of ~ 2.85 Å. The coordination sphere of the K^+ ions is completed by a single chelating en ligand. The K^+ ions chelated by $[\text{K}([2.2.2]\text{-crypt})]^+$ are separated from the centroid of the cluster by distances in excess of 7 Å. **2** (Figures S4 and S5) crystallises in the monoclinic space group $\text{P}2_1/c$ with three $[\text{K}(18\text{-Crown-6})]^+$ cations and one further, isolated, K^+ in the unit cell in addition to the $[(\text{CO})_3\text{MoSn}_5\text{Mo}(\text{CO})_3]^{4-}$ anion. The isolated K^+ cations form bridges between adjacent cluster units, in this case via three $\text{K}^+\text{-O}(\text{CO})$ contacts between 2.70 Å and 3.45 Å as well as three short $\text{K}^+\text{-Sn}$ contacts to the equatorial rings. These short $\text{K}^+\text{-Sn}$ contacts are responsible for the small distortion of the Sn_5 ring away from a perfect pentagon. The structures of the two anions are shown in Figure 2 and further details are given in Supporting Information, Figures S2–S5. The $[(\text{CO})_3\text{MSn}_5\text{M}(\text{CO})_3]^{4-}$ anions ($\text{M} = \text{Cr}$, **1**; Mo , **2**) are, like the Pb analogue [13], pentagonal bipyramids with a Sn_5 ring capped by two $\text{M}(\text{CO})_3$ fragments at the vertices. The $\text{M}\text{-M}$ distances along the principal axis are 2.948(9) Å and 3.1393(5) Å in **1** and **2**, respectively. Fässler and co-workers have emphasised the point that the Mo-Mo distance of 3.2156(8) Å in $[(\text{CO})_3\text{MPb}_5\text{M}(\text{CO})_3]^{4-}$ is longer than that in unambiguously Mo-Mo bonded species such as $[\text{Mo}_2(\text{CO})_{10}]^{2-}$ (Mo-Mo = 3.123 Å) [44]. The corresponding Mo-Mo distance of 3.1393(5) Å in the Sn_5 analogue, **2**, is,

however, almost identical to that in $[\text{Mo}_2(\text{CO})_{10}]^{2-}$ while the Cr–Cr distance of 2.948(9) Å in **1** is shorter than that in $[\text{Cr}_2(\text{CO})_{10}]^{2-}$, 2.970 Å [44]. The unambiguous identification of metal–metal bonds in systems with bridging ligands is notoriously difficult, as illustrated by the spirited debate over the existence or otherwise of an Fe–Fe bond in $\text{Fe}_2(\text{CO})_9$ [45–47], but in this case, it seems clear, at least, that direct metal–metal bonding cannot be excluded a priori based on the structural data alone. The Sn_5 rings are almost perfectly planar, with the sums of the interior angles close to the ideal value of 540° (**1**: 539.850° ; **2**: 539.928°). The Sn–Sn bond lengths in **1** (av. 2.878 Å) and **2** (av. 2.934 Å) (Figure 2) bracket the values in the Sn_5^{6-} clusters: 2.883 Å in Na_8EuSn_6 , 2.921 Å in Na_8BaSn_6 , again highlighting the absence of a simple relationship between bond length and formal charge [7].

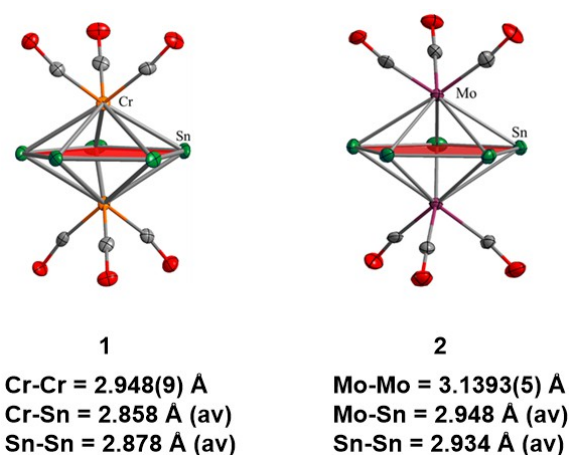


Figure 2. Molecular structure of the anions $[(\text{CO})_3\text{CrSn}_5\text{Cr}(\text{CO})_3]^{4-}$ and $[(\text{CO})_3\text{MoSn}_5\text{Mo}(\text{CO})_3]^{4-}$ in compounds **1** and **2**, respectively. Thermal ellipsoids are drawn at the 50% probability level.

3.2. ESI-MS

The ESI-MS of an acetonitrile solution of **1** shown in Figure 3 shows peaks at $m/z = 865.3735$ and 1281.5919 , identified as $[\text{Cr}_2\text{Sn}_5(\text{CO})_6]^-$ and $[\text{HK}(2.2.2\text{-crypt})\text{Cr}_2\text{Sn}_5(\text{CO})_6]^-$, respectively. No other small fragment peaks were found, indicating that compound **1** is relatively stable in acetonitrile solution under mass spectrometry conditions, albeit with a much reduced overall charge compared to the anion present in the crystal. Very similar features are apparent in the spectrum of **2** (Figures S6 and S7), where a prominent peak assigned to $[\text{K}(18\text{-Crown-6})\text{Mo}_2\text{Sn}_5(\text{CO})_6]^-$ is observed at $m/z \sim 1256$.

3.3. Electronic Structure Analysis

Optimised structural parameters for the two Sn_5 clusters $[(\text{CO})_3\text{MSn}_5\text{M}(\text{CO})_3]^{4-}$, $\text{M} = \text{Cr}, \text{Mo}$, are compared in Table 1, along with corresponding values for Fässler's Pb_5 cluster [13], using a range of exchange–correlation functionals. The gradient corrected functional (PBE) give somewhat shorter M–M bonds than their hybrid counterparts (B3LYP) [26], which is a relatively common observation in systems with weak metal–metal bonds [48]. In contrast, the double hybrid function B2PLYP [28,29] predicts M–M bond lengths that are shorter than any of the other functionals, and indeed even shorter than the experimental values. Despite the functional dependence of the absolute bond lengths, the calculations replicate the important trends in the crystallographic data, irrespective of functional. Within the pair of Sn_5 clusters, the optimised Cr–Cr bond length is ~ 0.2 Å shorter than the Mo–Mo bond and the Sn–Sn bonds in the Sn_5 ring are ~ 0.05 Å shorter in the Cr complex than its Mo counterpart. Likewise, the elongation of the Mo–Mo distance in $[\text{Mo}(\text{CO})_3\text{Pb}_5\text{Mo}(\text{CO})_3]^{4-}$ vs. $[(\text{CO})_3\text{MoSn}_5\text{Mo}(\text{CO})_3]^{4-}$ seen in the X-ray data is reproduced across all functionals.

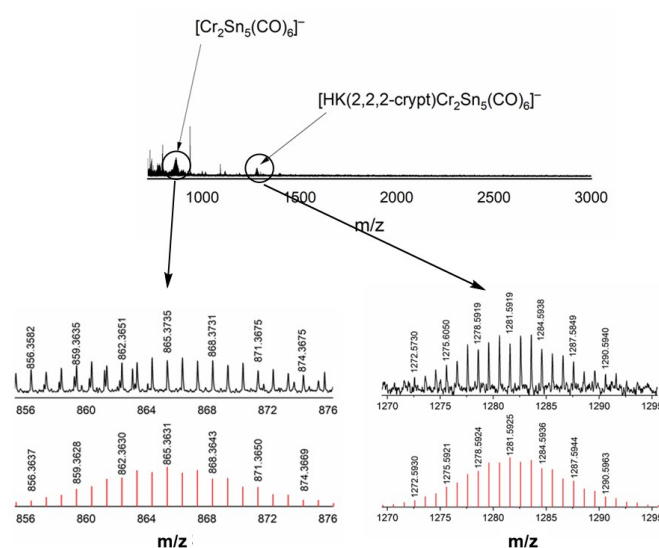


Figure 3. Negative-ion mode ESI-MS spectra of a freshly prepared solution of **1** in MeCN. The region of the spectrum corresponding to $[\text{Cr}_2\text{Sn}_5(\text{CO})_6]^-$ is expanded (Top: measured spectrum. Bottom: calculated spectrum).

Table 1. Optimised bond lengths for $[(\text{CO})_3\text{MSn}_5\text{M}(\text{CO})_3]^{4-}$, $\text{M} = \text{Cr}, \text{Mo}$ and $[(\text{CO})_3\text{MoPb}_5\text{Mo}(\text{CO})_3]^{4-}$ for PBE, B3LYP, M062X and B2PLYP functionals.

		M-M	M-Tt	Tt-Tt
$[(\text{CO})_3\text{CrSn}_5\text{Cr}(\text{CO})_3]^{4-}$	X-ray	2.95	2.86	2.88
	PBE	2.97	2.88	2.91
	B3LYP	3.07	2.91	2.91
	M062X	2.97	2.86	2.88
	B2PLYP	2.85	2.87	2.93
$[(\text{CO})_3\text{MoSn}_5\text{Mo}(\text{CO})_3]^{4-}$	X-ray	3.14	2.95	2.93
	PBE	3.19	2.99	2.98
	B3LYP	3.27	3.02	2.98
	M062X	3.20	2.97	2.95
	B2PLYP	3.15	2.98	2.97
$[(\text{CO})_3\text{MoPb}_5\text{Mo}(\text{CO})_3]^{4-}$	X-ray	3.21	3.05	3.04
	PBE	3.22	3.08	3.09
	B3LYP	3.31	3.11	3.10
	B2PLYP	3.17	3.06	3.09

A schematic molecular orbital diagram showing the interaction between a Sn_5^{4-} fragment and a $(\text{CO})_3\text{M}-\text{M}(\text{CO})_3$ unit is summarised in Figure 4. Quantitative versions for both clusters are shown in the Supporting Information, Figure S10. Note that the orbitals of the Sn_5^{4-} ring are labelled according to D_{5h} point symmetry while those of $\text{M}(\text{CO})_3$ and $(\text{CO})_3\text{M}-\text{M}(\text{CO})_3$ are labelled according to C_{3v} and D_{3h} , respectively. The complete cluster has only C_s point symmetry. The bonding interaction between the Sn_5^{4-} ring and the transition metal center is dominated by charge transfer from the highest occupied orbitals on Sn_5^{4-} with Sn-Sn σ (e'_1) and Sn-Sn π (e'_2) character, which overlap with in- and out-of-phase combinations of the degenerate LUMO of $\text{M}(\text{CO})_3$ ($2e'$ and $2e''$, respectively) to generate near-degenerate pairs with a' and a'' symmetry ($(5a', 3a'')$, $(6a', 4a'')$). The air- and moisture-sensitivity of both **1** and **2** has precluded the measurement of infra-red spectra for either, but our computed C-O stretching frequencies (1712 cm^{-1} and 1744 cm^{-1} for **1** and **2**, respectively) indicate a similar red-shift to that observed in the Pb_5 analogue (measured, 1737 cm^{-1} [13], calculated 1744 cm^{-1}). In addition, there is a further significant interaction between the out-of-phase combination of d_{z^2} orbitals and the $\text{Sn}_5 \pi a'_2$ orbital, which destabilises the antibonding combination to the extent that it constitutes the LUMO

of the complex ($8a'$). This LUMO, an iso-surface plot which is shown in Figure 4, is clearly localised primarily on the Sn_5 ring, with relatively minor contributions from the out-of-phase combination of Cr d_{z^2} orbitals.

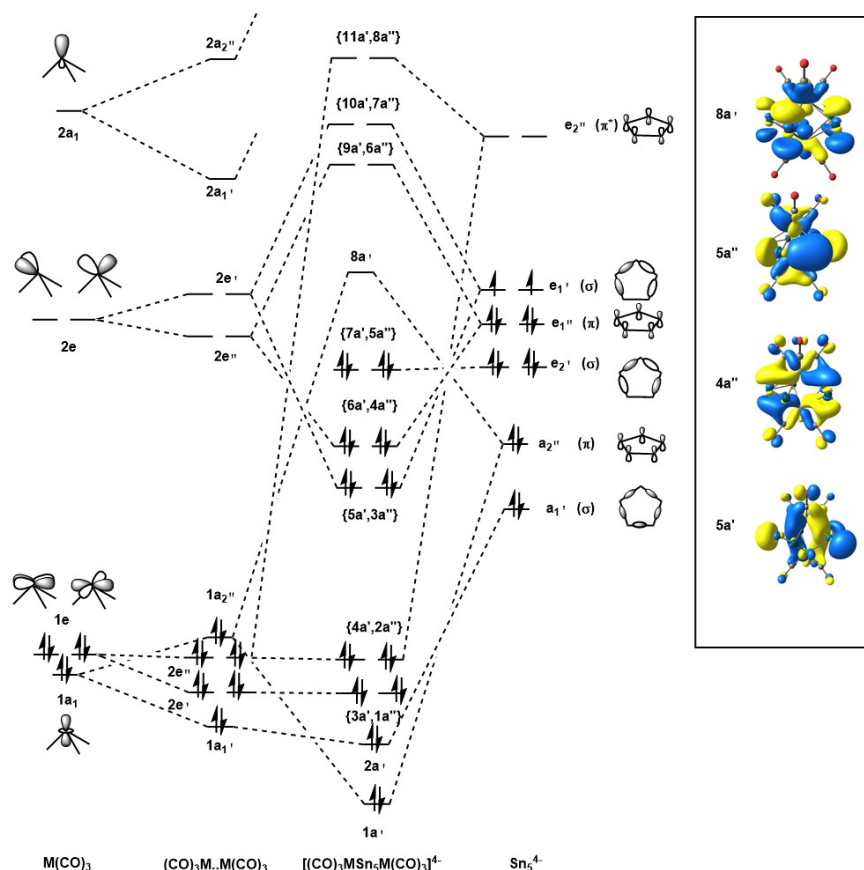


Figure 4. Schematic molecular orbital diagram for $[(\text{CO})_3\text{MSn}_5\text{M}(\text{CO})_3]^{4-}$. Note that the orbitals of the $\text{M}(\text{CO})_3$, $\text{M}_2(\text{CO})_6$ and Sn_5 fragments are labelled according to C_{3v} , D_{3h} and D_{5h} point symmetry, respectively. The cluster itself has only C_S point symmetry.

4. Discussion

Electron-Counting and Metal–Metal Bonding in Pentagonal Bipyramidal Clusters

In order to place these new Sn_5 clusters into an appropriate context, it is useful to compare them to other 7-vertex cluster compounds with the same or similar formal electron counts. A useful point of comparison is with the 7-vertex main-group clusters $\text{Tl}_4\text{Bi}_3^{3-}$ and Tl_7^{7-} , the former synthesised recently by Dehnen [49] and co-workers and the latter by Corbett and co-workers in 2000 [12]. The $[\text{Tl}_4\text{Bi}_3]^{3-}$ cluster has a total valence-electron count of $4n + 2 = 30$, a skeletal-electron count of $2n + 2 = 16$, and is a classically *closo* cluster with a distance of 4.086(3) Å between the two apical Tl atoms. Corbett's Tl_7^{7-} cluster, in contrast, has two electrons fewer ($4n = 28$) and is compressed along the principal axis, generating a short *trans*-annular Tl-Tl bond of 3.4622(9) Å. Its a_2'' -symmetric LUMO (the counterpart of which is occupied in $[\text{Tl}_4\text{Bi}_3]^{3-}$), shown in Figure 5, has Tl-Tl π^* character around the equator, just like the LUMOs of $[(\text{CO})_3\text{MSn}_5\text{M}(\text{CO})_3]^{4-}$, but also substantial Tl 6s character on the apical Tl atoms, and it is this feature that gives rise to the direct Tl-Tl bond [12,50].

How can we reconcile the well-established Wade's rules electron-counting model used in these main-group clusters with the electronic structure of $[(\text{CO})_3\text{MSn}_5\text{M}(\text{CO})_3]^{4-}$? Fässler and Kaupp formulated the skeletal electron count as $2n = 14$, treating the $\text{Mo}(\text{CO})_3$ fragment as a zero-electron donor. The assumption here is that the occupied $3d$ orbitals, including the $3d_{z^2}$ orbitals aligned along the principal axis, are not involved in the cluster bonding. The linear combinations of $3d_{z^2}$ are, however, the direct analogues of the $6s$ radial lone pairs in $[\text{Tl}_4\text{Bi}_3]^{3-}$, and if we do include these we reach a total-electron count of 28 ($=4n$), highlighting an isolobal analogy to Tl_7^{7-} . So why, then, do we consider a *trans*-annular Tl-Tl bond to be present in the main-group cluster, but not in $[(\text{CO})_3\text{MSn}_5\text{Cr}(\text{CO})_3]^{4-}$? The resolution to this question lies in the nature of the LUMO, and in particular its distribution over the five atoms of the equatorial ring and the two along the principal axis. To understand the significance of this orbital, we note that the hypothetical 30-electron (*closo*) clusters, $[(\text{CO})_3\text{MSn}_5\text{Cr}(\text{CO})_3]^{6-}$, can be formulated without ambiguity as a Sn_5^{6-} ring bridging two $\text{M}^0(\text{CO})_3$ fragments, with no *trans*-annular bond. If the LUMO of the 28-electron cluster is an out-of-phase combination of orbitals on the apical atoms, a *trans*-annular bond is fully developed while the equatorial five-membered ring retains the full complement of six π electrons. At the opposite extreme, if the LUMO is localised entirely in the equatorial plane, the electron deficiency is accommodated in an anti-aromatic 4π ring while both in- and out-of-phase combinations of $3d_{z^2}$ are occupied, annihilating the *trans*-annular bond. The LUMOs shown in Figure 5 suggest that the amplitude of the LUMO is indeed shifted towards the apical atoms in Tl_7^{7-} compared to $[(\text{CO})_3\text{CrSn}_5\text{Cr}(\text{CO})_3]^{4-}$, justifying the rather different descriptions of bonding applied in the two cases. An even more extreme example of a *trans*-annular bond can be found in the P_5 -bridged clusters, $\text{CpCrP}_5\text{CrCp}$ and $\text{Cp}^*\text{CrP}_5\text{CrCp}^*$ and their one-electron reduced analogues (Figure 1e) [14,51]. The neutral Cp cluster has a Cr-Cr separation is 2.69(1) Å, considerably shorter than that in **1**, and Hoffmann's analysis of the bonding [52] concludes that there is indeed Cr-Cr bonding present. The one-electron reduced analogue $[\text{CpCrP}_5\text{CrCp}]^-$ noted in Scherer's original report of the synthesis of the Cp^* compound [14] is particularly interesting in the present context because its total valence electron count of 28 establishes a further isolobal relationship to both Tl_7^{7-} and $[(\text{CO})_3\text{CrSn}_5\text{Cr}(\text{CO})_3]^{4-}$. The optimised structure of $[\text{CpCrP}_5\text{CrCp}]^-$ is summarised in Table 2, with full cartesian coordinates given in the Supplementary Materials: the Cr-Cr bond length of 2.61 Å is indicative of an even stronger Cr-Cr interaction than in the neutral species. The 28 available electrons in $[\text{CpCrP}_5\text{CrCp}]^-$ can either be partitioned to give a 6π -electron P_5^- ring and two d^5 CpCr fragments (and hence a Cr-Cr bond) or, alternatively, as a 4π -electron P_5^+ ring with two d^6 CpCr⁻ fragments (and hence no Cr-Cr bond). The LUMO, shown in Figure 5c, is clearly strongly localised on the apical Cr atoms with relatively minor contributions on the equatorial P_5 ring, confirming that the electron-deficiency is accommodated on the apical atoms.

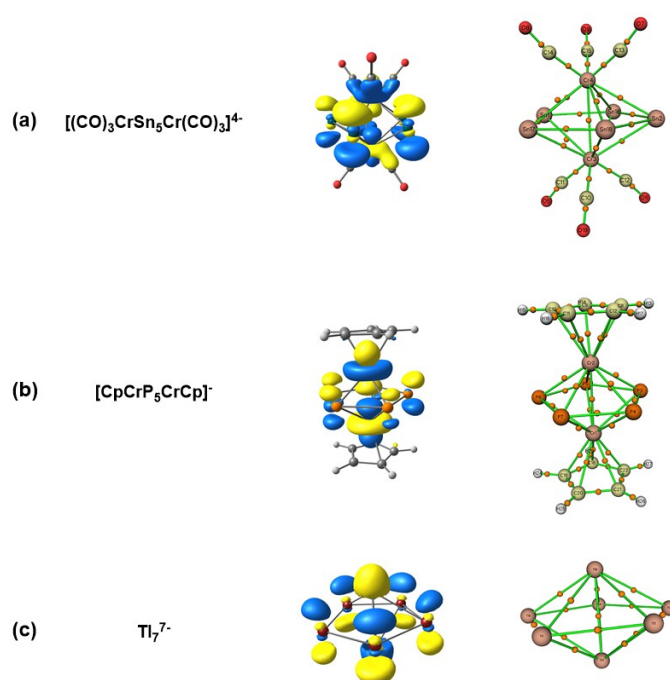


Figure 5. Contour plots of the LUMOs of (a) $[(\text{CO})_3\text{CrSn}_5\text{Cr}(\text{CO})_3]^{4-}$, (b) $[\text{CpCrP}_5\text{CrCp}]^-$ and (c) Tl_7^{7-} and the corresponding molecular graphs. Bond Critical Points (BCPs) are shown in the molecular graphs as orange dots.

An important point to take from this analysis is that there is no black-and-white distinction between the electronic structure models for $[(\text{CO})_3\text{CrSn}_5\text{Cr}(\text{CO})_3]^{4-}$, $[\text{CpCrP}_5\text{CrCp}]^-$ and Tl_7^{7-} . All three share a common skeletal-electron count of 28, two fewer than the *closo* count of 30, and they constitute a continuum of situations defined by the shape of the LUMO, and hence by the way that the electron deficiency (relative to the *closo* form) is accommodated. In terms of the molecular orbital diagram shown in Figure 4, the limiting cases defined by $[(\text{CO})_3\text{CrSn}_5\text{Cr}(\text{CO})_3]^{4-}$ and $[\text{CpCrP}_5\text{CrCp}]^-$ are connected by a shift in the relative energies of the metal- and E_5 -based fragments. A downward shift of the orbitals on the E_5 ring will increase the metal d_{z^2} character in the LUMO, increasing the importance of the *trans*-annular bonded resonance form while an upward shift increases the contribution of the anti-aromatic 4π configuration. The Quantum Theory of Atoms in Molecules (QTAIM) offers an alternative perspective on the nature of the bonding in these systems, although we note that the separation of metal–metal and metal–ligand bonding remains far from simple [53]. The delocalisation index, δ , offers a direct measure of Cr–Cr bond strength, and the values of 0.40 and 0.93 for $[(\text{CO})_3\text{CrSn}_5\text{Cr}(\text{CO})_3]^{4-}$ and $[\text{CpCrP}_5\text{CrCp}]^-$, respectively, correlate directly with the computed values for the Mayer bond order (0.39 and 0.72) extracted from the wavefunction itself (Table 2). A survey of the topology of the electron density identifies bond critical points (BCPs) midway between the Cr centres for both $[(\text{CO})_3\text{CrSn}_5\text{Cr}(\text{CO})_3]^{4-}$ and $[\text{CpCrP}_5\text{CrCp}]^-$ (see molecular graphs in Figure 5), but the electron density at the BCP (ρ_{BCP}) is considerably larger for the latter (0.055) than the former (0.028). Following Macchi’s classification of the local indicators of bond type [54], the balance between kinetic (G_b) and potential (V_b) energies is consistent with an open-shell-type interaction in both cases, although the local dominance of V_b over G_b in $[\text{CpCrP}_5\text{CrCp}]^-$ is indicative of enhanced covalent Cr–Cr character. All of the indicators, structural and electronic, are therefore consistent with the conclusion that Cr–Cr bonding is considerably stronger in $[\text{CpCrP}_5\text{CrCp}]^-$ than it is in $[(\text{CO})_3\text{CrSn}_5\text{Cr}(\text{CO})_3]^{4-}$. The Mayer bond order, delocalisation index and properties of the *trans*-annular BCP for the Tl_7^{7-} cluster suggest that it sits closer to $[(\text{CO})_3\text{CrSn}_5\text{Cr}(\text{CO})_3]^{4-}$ than to $[\text{CpCrP}_5\text{CrCp}]^-$ on this spectrum of bond types.

Table 2. Comparison of Mayer bond orders (BO) and QTAIM parameters for the *trans*-Annular M-M Bond Critical Points (BCPs) for 28-electron M_2E_5 clusters, $[(CO)_3CrSn_5Cr(CO)_3]^{4-}$, $[CpCrP_5CrCp]^-$, and Tl_7^{7-} .

	$[(CO)_3CrSn_5Cr(CO)_3]^{4-}$	$[CpCrP_5CrCp]^-$	Tl_7^{7-}
$r_{M-M}/\text{\AA}$	2.97	2.62	3.32
BO_{M-M}	0.39	0.72	0.31
δ_{M-M}	0.40	0.93	0.52
ρ_{BCP}/au	0.028	0.055	0.020
G_b/au	0.010	0.026	0.009
V_b/au	-0.015	-0.045	-0.010

5. Conclusions

In this paper we have reported the synthesis and structural characterisation of two new cluster compounds, $[(CO)_3MSn_5M(CO)_3]^{4-}$, $M = Cr, Mo$, which feature a pair of zerovalent $M(CO)_3$ fragments bridged by a *cyclo*- Sn_5 unit. The Sn clusters are isostructural with the Pb analogue, $[(CO)_3MoPb_5Mo(CO)_3]^{4-}$, reported previously by Fässler and co-workers. The LUMOs of both clusters have dominant Sn-Sn π character, consistent with their formulation as Sn_5^{4-} rings coordinated to two zero-valent $M(CO)_3$ fragments. The electronic structure makes a striking contrast with the isoelectronic $[CpCrP_5CrCp]^-$ anion, where the relative energies of the orbitals on the E_5 and M_2 fragments are reversed, causing the LUMO to have dominant Cr-Cr σ^* rather than Sn-Sn π character. The Tl_7^{7-} cluster is isolobal with both clusters, and the axial compression in this *hypo*-electronic cluster is strikingly reminiscent of the short Cr-Cr bond in $[CpCrP_5CrCp]^-$. These three 28-electron clusters therefore mark three distinct points on a continuum between two limits where (i) the LUMO is localised in the equatorial E_5 ring (as in $[(CO)_3MSn_5M(CO)_3]^{4-}$), and (ii) the LUMO is localised on the M_2 caps, forming a *trans*-annular bond (as in $[CpCrP_5CrCp]^-$). This continuum perspective establishes a link between apparently quite different electron-counting models.

Supplementary Materials: The following Supplementary Materials can be downloaded at: <https://www.mdpi.com/article/10.3390/inorganics10060075/s1>, Details of the crystallographic analysis (Figures S1–S5 and Tables S1 and S2), the ESI for **2** (Figures S6 and S7) and EDX (Figures S8 and S9) experiments. Cartesian coordinates of the optimized structures are given in Supporting Information, and quantitative MO diagrams for **1** and **2** are presented in Figure S10.

Author Contributions: Synthesis and characterization, W.-X.C. and Z.-M.S.; electronic structure analysis, S.M. and J.E.M. All authors have read and agreed to the published version of the manuscript.

Funding: This work was supported by the National Natural Science Foundation of China (92161102 and 21971118) and the Natural Science Foundation of Tianjin City (No. 20JCYBJC01560 and B2021202077). Z.M.S. thanks the 111 project (B18030) from China.

Data Availability Statement: Crystallographic data are available free of charge via www.ccdc.cam.ac.uk/data_requested/cif, entries CCDC-2122111 and CCDC-2122112 for compounds **1** and **2**, respectively (accessed on 15 November 2021).

Acknowledgments: S.M. acknowledges the Indian Government for a scholarship (National Overseas Scholarship).

Conflicts of Interest: The authors declare no conflict of interest.

Abbreviations

The following abbreviations are used in this manuscript:

DFT Density Functional Theory
 QTAIM Quantum Theory of Atoms in Molecules

References

1. Scherer, O.J. Complexes with Substituent-free Acyclic and Cyclic Phosphorus, Arsenic, Antimony, and Bismuth Ligands. *Angew. Chem. Int. Ed. Engl.* **1990**, *29*, 1104–1122. [[CrossRef](#)]
2. Turbervill, R.S.P.; Goicoechea, J.M. From Clusters to Unorthodox Pnictogen Sources: Solution-Phase Reactivity of $[E_7]^{3-}$ (E = P–Sb) Anions. *Chem. Rev.* **2014**, *114*, 10807–10828. [[CrossRef](#)]
3. Zhang, M.; Wang, W.; Sun, Z.; Meng, L.; Li, X. Construction of $Pn_{10}M$ Sandwich Compounds from Pn_5^- and Pn_5M (Pn = N–Bi; M = Li, Na, K, Be, Mg, Ca, Fe, Co and Ni): A Theoretical Assessment. *Comp. Theor. Chem.* **2016**, *1098*, 50–55. [[CrossRef](#)]
4. Dillon, K.B.; Mathey, F.; Nixon, J.F. *Phosphorus: The Carbon Copy*, 1st ed.; Wiley: New York, NY, USA, 1998.
5. Simpson, M.C.; Protasiewicz, J.D. Phosphorus as a Carbon Copy and as a Photocopy: New Conjugated Materials Featuring Multiply Bonded Phosphorus. *Pure App. Chem.* **2013**, *85*, 801–815. [[CrossRef](#)]
6. Heintl, C.; Peresykina, E.; Balázs, G.; Mädl, E.; Virovets, A.V.; Scheer, M. The Missing Parent Compound $[(C_5H_5)Fe(\eta^5-P_5)]$: Synthesis, Characterization, Coordination Behavior and Encapsulation. *Chem. Eur. J.* **2021**, *27*, 7542–7548. [[CrossRef](#)] [[PubMed](#)]
7. Todorov, I.; Sevov, S.C. Heavy-Metal Aromatic Rings: Cyclopentadienyl Anion Analogues Sn_5^{6-} and Pb_5^{6-} in the Zintl Phases Na_8BaPb_6 , Na_8BaSn_6 , and Na_8EuSn_6 . *Inorg. Chem.* **2004**, *43*, 6490–6494. [[CrossRef](#)] [[PubMed](#)]
8. von Schnering, H.G.; Nesper, R.; Curda, J.; Tebbe, K.F. $Li_{12}Si_7$, a Compound Having a Trigonal Planar Si_4 Cluster and Planar Si_5 Rings. *Angew. Chem. Int. Ed. Engl.* **1980**, *19*, 1033–1034. [[CrossRef](#)]
9. Nesper, R.; Curda, J.; Von Schnering, H. Li_8MgSi_6 , a Novel Zintl Compound Containing Quasi-Aromatic Si_5 rings. *J. Solid State Chem.* **1986**, *62*, 199–206. [[CrossRef](#)]
10. Frank, U.; Müller, W. $Li_{11}Ge_6$ —A Phase with Isolated, Plane, Five-Membered Ge-Rings. *Z. Naturf. B* **1975**, *30*, 313–315. [[CrossRef](#)]
11. Wade, K. Structural Significance of Number of Skeletal Bonding Electron-Pairs in Carboranes, Higher Boranes and Borane Anions, and Various Transition-Metal Carbonyl Cluster Compounds. *J. Chem. Soc. D Chem. Comm.* **1971**, *15*, 792–793. [[CrossRef](#)]
12. Kaskel, S.; Corbett, J.D. Synthesis and Structure of $K_{10}Tl_7$: The First Binary Trielide Containing Naked Pentagonal Bipyramidal Tl_7 Clusters. *Inorg. Chem.* **2000**, *39*, 778–782. [[CrossRef](#)]
13. Yong, L.; Hoffmann, S.D.; Fässler, T.F.; Riedel, S.; Kaupp, M. $[Pb_5[Mo(CO)_3]_2]^{4-}$: A complex containing a planar Pb_5 unit. *Ang. Chem. Int. Ed. Engl.* **2005**, *44*, 2092–2096. [[CrossRef](#)]
14. Scherer, O.J.; Schwab, J.; Wolmershäuser, G.; Kaim, W.; Gross, R. *cyclo-P₅* as Complex Ligand—The Phosphorus Analogue of the Cyclopentadienyl Ligand. *Angew. Chem. Int. Ed. Engl.* **1986**, *25*, 363–364. [[CrossRef](#)]
15. Armstrong, R.S.; Aroney, M.J.; Barnes, C.M.; Nugent, K.W. Infrared and Raman Spectra of $(\eta^6\text{-mesitylene})M(CO)_3$ Complexes (M = Cr, Mo or W): An Insight Into Metal-Arene Bonding. *App. Organomet. Chem.* **1990**, *4*, 569–580. [[CrossRef](#)]
16. Gholiee, Y.; Salehzadeh, S.; Khodaveisi, S. Significant Geometry and Charge Difference Between the E_5^{4-} Bare Clusters of Group 14 Zintl anions and Their Coordinated Form in $[E_5[M(CO)_3]_2]^{4-}$ (E = Si, Ge, Sn, Pb; M = Cr, Mo, W) complexes. *New J. Chem.* **2019**, *43*, 7797–7805. [[CrossRef](#)]
17. Tate, D.P.; Knipple, W.R.; Augl, J.M. Nitrile Derivatives of Chromium Group Metal Carbonyls. *Inorg. Chem.* **1962**, *1*, 433–434. [[CrossRef](#)]
18. Sheldrick, G.M. SHELXT—Integrated Space-Group and Crystal-Structure Determination. *Acta Cryst. Section A* **2015**, *71*, 3–8. [[CrossRef](#)]
19. Dolomanov, O.V.; Bourhis, L.J.; Gildea, R.J.; Howard, J.A.K.; Puschmann, H. OLEX2: A Complete Structure Solution, Refinement and Analysis Program. *J. App. Cryst.* **2009**, *42*, 339–341. [[CrossRef](#)]
20. Spek, A.L. PLATON SQUEEZE: A Tool for the Calculation of the Disordered Solvent Contribution to the Calculated Structure Factors. *Acta Cryst. Section C* **2015**, *71*, 9–18. [[CrossRef](#)]
21. Neese, F. The ORCA Program System. *Wiley Interdiscip. Rev. Comput. Mol. Sci.* **2012**, *2*, 73–78. [[CrossRef](#)]
22. Neese, F. Software Update: The ORCA Program System, Version 4.0. *Wiley Interdiscip. Rev. Comput. Mol. Sci.* **2018**, *8*, e1327. [[CrossRef](#)]
23. Perdew, J.P.; Burke, K.; Ernzerhof, M. Generalized Gradient Approximation Made Simple. *Phys. Rev. Lett.* **1996**, *77*, 3865–3868. [[CrossRef](#)] [[PubMed](#)]
24. Becke, A.D. Density-Functional Thermochemistry. III. The Role of Exact Exchange. *J. Chem. Phys.* **1993**, *98*, 5648–5652. [[CrossRef](#)]
25. Lee, C.; Yang, W.; Parr, R.G. Development of the Colle-Salvetti Correlation-Energy Formula into a Functional of the Electron Density. *Phys. Rev. B* **1988**, *37*, 785. [[CrossRef](#)]
26. Hertwig, R.H.; Koch, W. On the Parameterization of the Local Correlation Functional. What is Becke-3-LYP? *Chem. Phys. Lett.* **1997**, *268*, 345–351. [[CrossRef](#)]
27. Zhao, Y.; Truhlar, D.G. The M06 Suite of Density Functionals for Main Group Thermochemistry, Thermochemical Kinetics, Noncovalent Interactions, Excited States, and Transition Elements: Two New Functionals and Systematic Testing of Four M06-Class Functionals and 12 Other Functionals. *Theor. Chem. Acc.* **2008**, *120*, 215–241.
28. Grimme, S. Semiempirical Hybrid Density Functional with Perturbative Second-Order Correlation. *J. Chem. Phys.* **2006**, *124*, 034108. [[CrossRef](#)]
29. Neese, F.; Schwabe, T.; Grimme, S. Analytic Derivatives for Perturbatively Corrected “Double Hybrid” Density Functionals: Theory, Implementation, and Applications. *J. Chem. Phys.* **2007**, *126*, 124115. [[CrossRef](#)]
30. van Lenthe, E.; Baerends, E.J.; Snijders, J.G. Relativistic Regular Two-Component Hamiltonians. *J. Chem. Phys.* **1993**, *99*, 4597–4610. [[CrossRef](#)]

31. van Lenthe, E.; Baerends, E.J.; Snijders, J.G. Relativistic Total Energy Using Regular Approximations. *J. Chem. Phys.* **1994**, *101*, 9783–9792. [[CrossRef](#)]
32. van Lenthe, E.; Ehlers, A.; Baerends, E.J. Geometry Optimizations in the Zero Order Regular Approximation for Relativistic Effects. *J. Chem. Phys.* **1999**, *110*, 8943–8953. [[CrossRef](#)]
33. Weigend, F.; Ahlrichs, R. Balanced Basis Sets of Split Valence, Triple Zeta Valence and Quadruple Zeta Valence Quality for H to Rn: Design and Assessment of Accuracy. *Phys. Chem. Chem. Phys.* **2005**, *7*, 3297–3305. [[CrossRef](#)]
34. Rolfes, J.D.; Neese, F.; Pantazis, D.A. All-Electron Scalar Relativistic Basis Sets for the Elements Rb–Xe. *J. Comp. Chem.* **2020**, *41*, 1842–1849. [[CrossRef](#)]
35. Pantazis, D.A.; Neese, F. All-Electron Scalar Relativistic Basis Sets for the 6p Elements. *Theor. Chem. Acc.* **2012**, *131*, 1292. [[CrossRef](#)]
36. Weigend, F. Accurate Coulomb-fitting Basis Sets for H to Rn. *Phys. Chem. Chem. Phys.* **2006**, *8*, 1057–1065. [[CrossRef](#)]
37. Klamt, A.; Schüürmann, G. COSMO: A New Approach to Dielectric Screening in Solvents with Explicit Expressions for the Screening Energy and its Gradient. *J. Chem. Soc. Perkin Trans.* **1993**, *2*, 799–805. [[CrossRef](#)]
38. Andzelm, J.; Kölmel, C.; Klamt, A. Incorporation of Solvent Effects into Density Functional Calculations of Molecular Energies and Geometries. *J. Chem. Phys.* **1995**, *103*, 9312–9320. [[CrossRef](#)]
39. Barone, V.; Cossi, M. Quantum Calculation of Molecular Energies and Energy Gradients in Solution by a Conductor Solvent Model. *J. Phys. Chem. A* **1998**, *102*, 1995–2001. [[CrossRef](#)]
40. Cossi, M.; Rega, N.; Scalmani, G.; Barone, V. Energies, Structures, and Electronic Properties of Molecules in Solution with the C-PCM Solvation Model. *J. Comp. Chem.* **2003**, *24*, 669–681. [[CrossRef](#)]
41. Lu, T.; Chen, F. Multiwfn: A Multifunctional Wavefunction Analyzer. *J. Comp. Chem.* **2012**, *33*, 580–592. [[CrossRef](#)]
42. Zhurko G. A. Chemcraft—Graphical Program for Visualization of Quantum Chemistry Computations. Ivanovo, Russia, 2005. Available online: <https://chemcraftprog.com> (accessed on 15 November 2021).
43. Kesanli, B.; Fettingner, J.; Eichhorn, B. The *closo*-[Sn₉M(CO)₃]⁴⁻ Zintl Ion Clusters where M = Cr, Mo, W: Two Structural Isomers and Their Dynamic Behavior. *Chem. Eur. J.* **2001**, *7*, 5277–5285. [[CrossRef](#)]
44. Handy, L.B.; Ruff, J.K.; Dahl, L.F. Structural Characterization of the Dinuclear Metal Carbonyl Anions [M₂(CO)₁₀]²⁻ (M = chromium, molybdenum) and [Cr₂(CO)₁₀H]⁻. Marked Stereochemical Effect of a Linearly Protonated Metal-Metal Bond. *J. Am. Chem. Soc.* **1970**, *92*, 7312–7326. [[CrossRef](#)]
45. Green, J.C.; Green, M.L.H.; Parkin, G. The Occurrence and Representation of Three-Centre Two-Electron Bonds in Covalent Inorganic Compounds. *Chem. Commun.* **2012**, *48*, 11481–11503. [[CrossRef](#)]
46. Labinger, J.A. Does Cyclopentadienyl Iron Dicarboxyl Dimer Have a Metal–Metal bond? Who’s Asking? *Inorg. Chim. Acta* **2015**, *424*, 14–19. [[CrossRef](#)]
47. McGrady, J.E. *Molecular Metal-Metal Bonds: Compounds, Synthesis, Properties*; Wiley: New York, NY, USA, 1999.
48. Spivak, M.; Arcisauskaitė, V.; López, X.; McGrady, J.E.; de Graaf, C. A Multi-Configurational Approach to the Electronic Structure of Trichromium Extended Metal Atom Chains. *Dalton Trans.* **2017**, *46*, 6202–6211. [[CrossRef](#)]
49. Lichtenberger, N.; Franzke, Y.J.; Massa, W.; Weigend, F.; Dehnen, S. The Identity of “Ternary” A/Tl/Pb or K/Tl/Bi Solid Mixtures and Binary Zintl Anions Isolated From Their Solutions. *Chem. Eur. J.* **2018**, *24*, 12022–12030. [[CrossRef](#)]
50. McGrady, J.E. A Unified Approach to Electron Counting in Main-Group Clusters. *J. Chem. Ed.* **2004**, *81*, 733. [[CrossRef](#)]
51. Goh, L.Y.; Wong, R.C.S.; Chu, C.K.; Hambley, T.W. Reaction of [(Cr(cp)(CO)₃)₂] (cp = η⁵-C₅H₅) with Elemental Phosphorus. Isolation of [Cr₂(cp)₂(P₃)] as a Thermolysis Product and its X-ray Crystal Structure. *J. Chem. Soc. Dalton Trans.* **1990**, *3*, 977–982
52. Tremel, W.; Hoffmann, R.; Kertesz, M. Inorganic Rings, Intact and Cleaved, Between Two Metal Fragments. *J. Am. Chem. Soc.* **1989**, *111*, 2030–2039. [[CrossRef](#)]
53. Lepetit, C.; Fau, P.; Fajerweg, K.; Kahn, M.L.; Silvi, B. Topological Analysis of the Metal-Metal Bond: A Tutorial Review. *Coord. Chem. Rev.* **2017**, *345*, 150–181. [[CrossRef](#)]
54. Macchi, P.; Proserpio, D.M.; Sironi, A. Experimental Electron Density in a Transition Metal Dimer: Metal-Metal and Metal-Ligand Bonds. *J. Am. Chem. Soc.* **1998**, *120*, 13429–13435. [[CrossRef](#)]